First-principles study of structural, electronic and optical properties of BaF_2 in its cubic, orthorhombic and hexagonal phases

2003 J. Phys.: Condens. Matter 15 709

(http://iopscience.iop.org/0953-8984/15/4/310)

INSTITUTE OF PHYSICS PUBLISHING JOURNAL OF PHYSICS: CONDENSED MATTER

J. Phys.: Condens. Matter **15** (2003) 709–718 PII: S0953-8984(03)54775-0

First-principles study of structural, electronic and optical properties of BaF_2 in its cubic, orthorhombic and hexagonal phases

Huitian Jiang[1], **Ravindra Pandey**[1], **Clovis Darrigan**[2] **and Michel Rérat**[2]

[1] Department of Physics, Michigan Technological University, Houghton, MI 49931, USA
[2] Laboratoire de Chimie Structurale, Universite de Pau, France

Received 15 October 2002
Published 20 January 2003
Online at stacks.iop.org/JPhysCM/15/709

Abstract

We present the results of a first-principles study on BaF_2 in its stable (cubic) and high-pressure phases. A linear combination of atomic orbitals approach in the framework of density functional theory is employed for total energy calculations in cubic, orthorhombic and hexagonal phases of BaF_2. A fitting of the energy surface to the equation of state yields the lattice constant and the bulk modulus of these phases at zero pressure which are in good agreement with the corresponding experimental values. Analysis of band structure determines the high-pressure phases to be direct-gap materials and no metallization of BaF_2 is predicted to occur for pressures up to 50 GPa. Furthermore, several peaks observed in the spectroscopic experiments have been identified with interband transitions in the cubic BaF_2. The calculated mean value of the refractive index is found to increase in going from the cubic to orthorhombic to hexagonal phases of BaF_2.

1. Introduction

Barium fluoride (BaF_2) is an important member of alkaline-earth fluorides and has been extensively studied for its intrinsic optical properties [1–3]. Specifically, it is the fastest luminescent material that has been found to date [4], thereby making it an ideal high-density luminescent material for applications in gamma ray and elementary particle detectors [5]. Recently, BaF_2 has also been found to exhibit superionic conductivity by dissolving appropriate impurities into the lattice or by introducing an interface that causes the redistribution of ions in the space-charge region [6], and is therefore considered as a candidate material for high-temperature batteries, fuel cells, chemical filters and sensors [6].

In 1972, Rubloff [7] reported the results of a detailed study of far-ultraviolet reflectance spectra of ionic crystals including BaF_2, using synchrotron radiation as a light source. The spectrum was composed of a number of strong peaks ranging from 10 to 20 eV which were assigned to electronic excitations in the material. In the subsequent experimental studies using

characteristic energy loss spectra [8], photoelectron spectroscopy [9, 10], x-ray absorption [11] and two-photon absorption spectra [12], the results more or less confirmed the existence of excitation peaks observed first in the reflectance spectra. The observed BaF_2 electronic excitation peaks were then interpreted by comparing the results with those available for KCl and CaF_2 [13, 14] due to the absence of any theoretical studies on BaF_2. This led to ambiguity in the peak assignments of the excitation spectrum of BaF_2 [7–9, 11, 15]. For example, the band-edge at about 10 eV was attributed to excitations associated with either Γ or X in the band structure of BaF_2, though it is well accepted that the top of the valence band is mainly formed by F 2p orbitals and the bottom of the conduction band consists of Ba cationic orbitals [9].

Surprisingly, after about 30 years, ambiguity about the assignment of the band-edge excitation and other peaks in the reflectance spectra of BaF_2 still persists. This is in spite of the fact that first-principles calculations with proven predictive capabilities are now routinely performed on a wide variety of materials to gain an understanding of their structural, thermodynamic, electronic and optical properties [16, 17]. It should be noted here that defects processes involving vacancies [18, 19], interstitials [19, 20], oxygen [21] and cerium in BaF_2 [22] have been investigated employing both atomistic and embedded quantum cluster techniques. Although Ching *et al* [23] have reported the band structure of BaF_2, the focus of their study was calculations of linear and nonlinear susceptibilities of ionic crystals. We will comment on the results of this somewhat limited study on the band structure of BaF_2 in section 4.

At ambient conditions, BaF_2 crystallizes in the cubic phase with a space group of $Fm3m$ (C1) [24, 25]. The high-pressure induced phase transition to the orthorhombic phase (space group $Pnma$ (C23)) is reported to occur at 3–5 GPa [24–27]. Furthermore, at about 10–15 GPa, BaF_2 undergoes a phase transition to the hexagonal phase [25] ($P6_3mmc$ ($B8_b$)) [25, 28]. Except for the experimental work on structural properties of these high-pressure phases of BaF_2, we are not aware of any theoretical or experimental studies revealing the electronic and optical properties of these high-pressure phases of BaF_2 in the literature.

In the present study, we report the results of a comprehensive theoretical investigation of BaF_2 in the cubic and high-pressure orthorhombic and hexagonal phases. Our aim will be

(i) to provide detailed information on electronic and optical properties,
(ii) to determine the equation of state and
(iii) to combine knowledge of the electronic structure and the equation of state to determine the effect of pressure on the electronic structure.

The rest of the paper is organized as follows. In section 2, we briefly describe the computational techniques used in this work. Results and discussion of the structural, electronic and optical properties will be presented in sections 3–5, and a summary of the work will be given in section 6.

2. Computational method

All-electron density functional theory (DFT) calculations were performed in the framework of the periodic linear combination of atomic orbitals (LCAO) approximation. In the LCAO–DFT approximation, a linear combination of Gaussian orbitals is used to construct a localized atomic basis from which Bloch functions are constructed by a further linear combination with plane-wave phase factors. The Gaussian basis sets used in the present study are seven s, six p and three d-type shells for Ba (i.e. a 9763111/ 763111/ 631 set) and seven s, six p and three d-type shells for F (i.e. a 9763111/ 763111/ 631 set). The basis set for fluorine was taken from

the LCAO–DFT study of electronic structure of CaF_2 [29]. For the basis set of barium, we began with the ionic basis set [30] for barium (i.e. Ba^{2+}) realizing that Ba in BaF_2 is expected to be fully ionic. Additional diffuse and polarization functions of s-, p- and d-type shells were then added to the ionic basis set. The exponents of these additional functions were optimized at the experimental geometry of BaF_2 by performing total energy calculations. The complete basis set of barium used in this study can be obtained from the authors (pandey@mtu.edu).

For calculations, we used gradient-corrected functionals (GGA), Becke [31] for exchange and Perdew and Wang [32] for correlation as implemented in the program package CRYSTAL98 [33]. The tolerance on the total energy convergence in the iterative solution of the Kohn–Sham equations is set to 10^{-6} Hartree and a grid of 50 k-points is used in the irreducible Brillouin zone for integration in the reciprocal space. Overall, the residual numerical uncertainty is estimated to be about 0.01 eV/atom.

3. Structural properties

The cubic phase is the stable phase of BaF_2 at ambient conditions. It undergoes a high-pressure phase transition to an orthorhombic phase at about 5 GPa and then to a hexagonal phase between 10 and 15 GPa. Above 17 GPa, BaF_2 exists only in the hexagonal phase [25]. It is to be noted here that the high-pressure phase transition from the cubic phase to the orthorhombic phase is accompanied by a large hysteresis, making the orthorhombic phase metastable at zero pressure. The phase transition from the orthorhombic phase to the hexagonal phase is also accompanied by hysteresis [25].

The cubic phase has only one free parameter, a, the length of the cell, since all ions are occupying fixed special positions in the unit cell. Thus, each point in the potential energy surface (i.e. $E(V)$ curve) of the cubic phase requires a single calculation with no optimization of the internal parameters of the unit cell. Figure 1 displays the calculated energy surface of the cubic BaF_2 which is fitted to Vinet's equation of state [34] to obtain lattice constant a, bulk modulus B and its pressure derivative B'. Accordingly, the calculated values of a, B and B' are 6.32 Å, 58.5 GPa and 4.91, respectively, while the measured values of a, B and B' are 6.20 Å, 57 GPa and 4, respectively [25]. Overall, the agreement between the calculated and experimental values is very good; both lattice constant and bulk modulus are within 1% of the respective experimental values. The calculated binding energy of -24.46 eV for the cubic BaF_2 is in good agreement with the experimental value of -24.38 eV. The experimental value of the binding energy was obtained from the application of the Born–Fajans–Haber cycle [35], using thermochemical data [36, 37].

The orthorhombic (C23) phase has two independent variables (i.e. b/a and c/a) for a fixed unit cell volume [38]. Its unit cell has six internal parameters (i.e. x_{Ba}, z_{Ba}, x_{F_1}, z_{F_1}, x_{F_2} and z_{F_2}) that need to be optimized. Total energy optimization of the C23 phase therefore requires the optimization of six internal variables together with b/a and c/a for each point on the potential energy surface. However, we have taken a rather simpler approach assuming a very small variation in the internal parameters with respect to the pressure up to 20 GPa. Using this approach, we first optimize the six internal coordinates at the experimental equilibrium volume of the orthorhombic BaF_2. For unit cell volumes different from the experimental one, we freeze the internal coordinates and optimize only b/a and c/a for each point on the potential energy surface. Under these constraints, the calculated internal parameters for the orthorhombic unit cell compare well with the corresponding experimental values. The calculated (experimental) values of these parameters are as follows: $x_{Ba} = 0.245(0.259)$, $z_{Ba} = 0.110(0.112)$, $x_{F_1} = 0.848(0.861)$, $z_{F_1} = 0.074(0.067)$, $x_{F_2} = 0.471(0.461)$ and $z_{F_2} = 0.822(0.820)$.

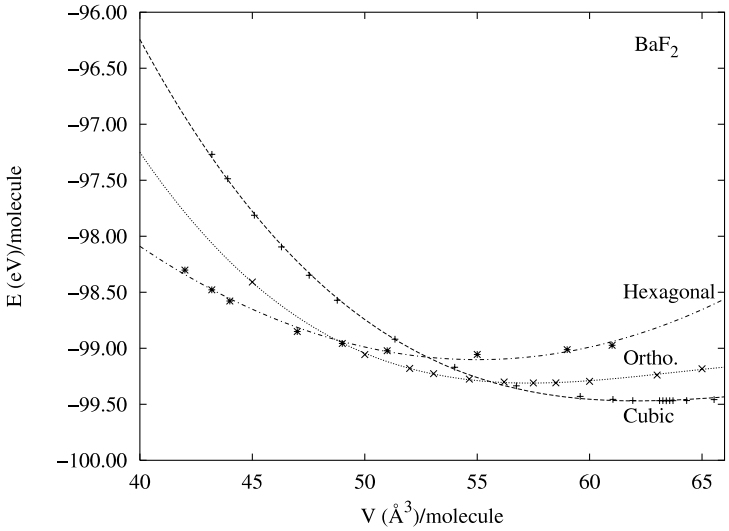

Figure 1. Total energy ($-219\,800$ eV$+E$) versus volume of BaF_2 in the cubic, orthorhombic and hexagonal phases.

Table 1. Structural properties of the cubic, orthorhombic and hexagonal phases of BaF_2 at zero pressure. V_0 is the volume of the cubic phase BaF_2.

	Cubic (C1)	Orthorhombic (C23)	Hexagonal ($B8_b$)
V/V_0	1	0.914	0.857
a (Å)	6.32	6.871	4.501
b/a	—	0.608	—
c/a	—	1.174	1.373

Figure 1 shows the generated potential energy surface of the orthorhombic BaF_2 with a minimum at 62.70 Å^3/molecule at zero pressure. Relative to the unit cell volume of the stable cubic phase, the calculated volume of the (metastable) orthorhombic phase turns out to be 0.914 which is in excellent agreement with the corresponding experimental [25] value of 0.907 (see table 1).

For the high-pressure hexagonal BaF_2, there are two independent variables (i.e. a *and* c/a) for a fixed unit cell volume [38]. The potential energy surface shown in figure 1 is calculated by optimizing both variables for each volume. At zero pressure, the equilibrium unit cell volume of the hexagonal phase relative to that of the cubic phase turns out to be 0.857. The values of a and c corresponding to the equilibrium volume are 4.501 and 6.180 Å. We note here that the lattice constants of the hexagonal BaF_2 were obtained at 20.5 GPa using high-pressure x-ray diffraction experiments. To facilitate a comparison of calculations with experiments, we have performed the optimization of a and c/a for the unit cell volume corresponding to 20.5 GPa for the hexagonal BaF_2. The optimized values of a and c turn out to be 4.283 and 5.469 Å, in good agreement with the experimental values [25] of 4.253 and 5.516 Å, respectively.

In a recent high-pressure x-ray and neutron-diffraction study [25] of BaF_2, phase transitions from cubic to orthorhombic and hexagonal phases were observed at about 3–5 and 10–15 GPa, respectively. In this study, the pressure corresponding to a phase transition from cubic to orthorhombic (hexagonal) was calculated by imposing the equilibrium condition of an equal Gibbs function for the cubic and orthorhombic (hexagonal) phases. The calculated

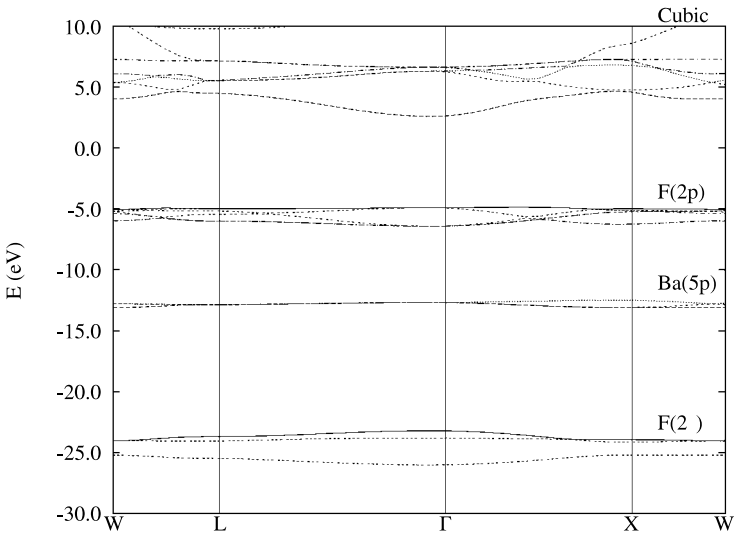

Figure 2. Electronic band structure of the cubic BaF_2.

values of the pressure corresponding to a phase transition from cubic to orthorhombic and hexagonal phase turn out to be 5.1 and 11.2 GPa, respectively, in agreement with experiments.

The bulk modulus of the cubic BaF_2 shows an increase with the pressure up to 5 GPa. Its values for the high-pressure orthorhombic and the hexagonal phases are calculated to be 98 and 142 GPa. The respective values obtained from the high-pressure measurements are 82 ± 10 and 133 ± 16 GPa for the orthorhombic and the hexagonal phases [25].

4. Electronic structure

The valence and conduction band structure of the cubic BaF_2 is displayed in figure 2 where anionic and cationic states are expected to constitute the top of the valence band and the bottom of the conduction band, respectively. Accordingly, the F 2p states form the upper valence band, followed by a band due to the Ba 5p states at about 7.8 eV below the top of the valence band. The F 2s states form a band at about 18.3 eV below the top of the valence band whereas the band formed by the Ba 5s states is at about 21.1 eV below the top of the valence band. It is to be noted here that the Ba 5s band is not shown in figure 2. Interestingly, calculations yield a location of the outermost core band (due to the Ba 5p states) in excellent agreement with the reflection and photoelectron experiments which report the band to be at about 7.8 eV below the valence band [12, 39]. It is to be noted here that calculations based on DFT provide a very good description of electronic states in the valence band, though they are not as reliable in describing the conduction states.

In the absence of the spin–orbit interaction terms in these calculations, the top of the valence band consists of the triply degenerate Γ_{15} level. The minimum of the conduction band is found to be at Γ (i.e Γ_1^c), which is lower than that at X (i.e. X_1^c) (see table 2). Thus, the present GGA calculations predict BaF_2 to be a direct-gap material with the bandgap of 7.5 eV. The experimental value of the gap is reported to be 11.0 eV. It is well known that DFT-based calculations underestimate the bandgap which may be corrected by employing a

Table 2. Direct and indirect DFT energy gaps of the cubic, orthorhombic and hexagonal phases of BaF_2 at zero pressure. An empirical expression (see equation (1)) is applied to correct the DFT energy gaps.

		Cubic (C1)		Orthorhombic (C23)		Hexagonal ($B8_b$)	
Bandgap (eV)		DFT	Corrected	DFT	Corrected	DFT	Corrected
Direct	Γ	7.49	11.64	Γ 7.36	11.55	Γ 6.0	10.15
	X	9.66	13.81	X 8.55	12.75	M 7.29	11.44
	L	9.48	13.63	R 8.96	13.15	L 7.56	11.71
Indirect	X–Γ	7.58	11.73	X–Γ 7.42	11.61	M–Γ 6.13	10.28
	L–Γ	7.57	11.72	R–Γ 7.49	11.68	L–Γ 6.37	10.52
	Pressure coefficients of the cubic phase, $\times 10^{-6}$ eV bar^{-1}						
Valence band	Γ_{15}	6.28					
	X_5	7.93					
	L'_3	7.76					
Conduction band	Γ_1	15.38					
	X_1	10.60					
	L'_2	17.89					

semi-empirical correction [40]. It uses the following equation:

$$\Delta \approx \frac{9\,\mathrm{eV}}{\varepsilon_\infty} \tag{1}$$

where ε_∞ is 2.17, the high-frequency dielectric constant of BaF_2 [41]. This semi-empirical correction simply shifts the levels in the conduction band, yielding the value of the gap as 11.6 eV, in a good agreement with the corresponding experimental value of 11.0 eV. Detailed results are listed in table 2. Previously, calculations based on orthogonalized LCAO in the local-density approximation (OLCAO–LDA) reported [23] the top of the valence band to be dispersive with the bottom of the conduction band at X. The focus of this study was calculations of linear and non-linear susceptibilities in alkali halides, alkaline-earth oxides, sulfides and fluorides. It therefore did not give the details of band structure and interband transitions in the cubic BaF_2 [23].

Both valence and conduction levels in the cubic BaF_2 are found to be sensitive to applied hydrostatic pressure. The calculated pressure coefficients are also listed in table 2. It is expected that knowledge of the pressure coefficients for different levels would assist experimentalists in identifying various optical transitions in the cubic BaF_2.

Electronic structure calculations find the metastable orthorhombic BaF_2 and the hexagonal BaF_2 to be a direct gap material at zero pressure (see table 2). Figures 3 and 4 display a few selected valence and conduction bands of the orthorhombic and hexagonal phases, respectively. At the transition pressure where the pressure-induced phase transition occurs, the minimum energy gap remains direct in both orthorhombic and hexagonal phases. Calculations do not predict closing of the energy gap up to 50 GPa in the hexagonal BaF_2, thus confirming the experimental observation of no metallization occurring in BaF_2 at such high pressures [25].

5. Optical properties

The satellite peaks due to the interband transitions in the cubic BaF_2 have been identified by several experimental techniques including the reflectance spectra [7], characteristic energy loss

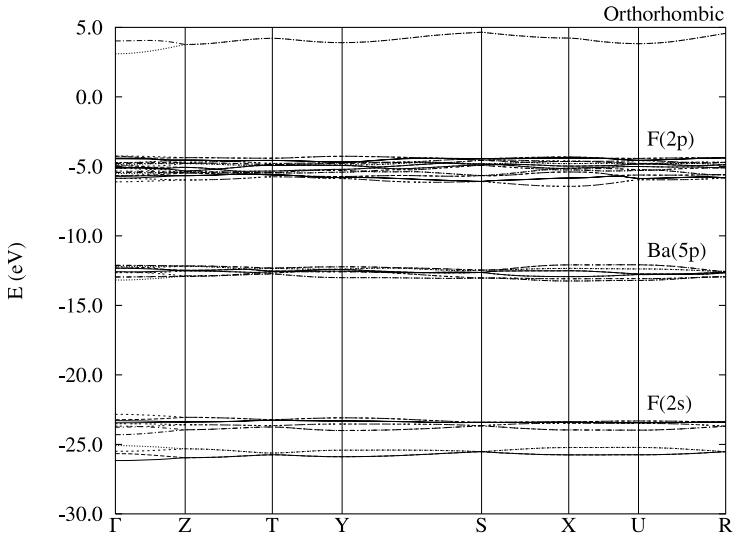

Figure 3. Electronic band structure of the orthorhombic BaF_2.

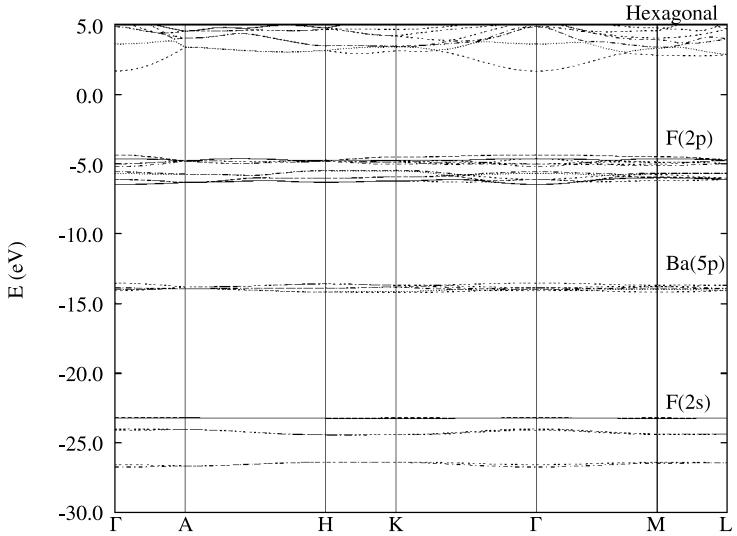

Figure 4. Electronic band structure of the hexagonal BaF_2.

spectra [8], and x-ray photoelectron spectroscopy [9]. All of these experimental measurements are in agreement in classifying the satellite peaks into two groups originating either from the upper valence band (F 2p) or the outermost core band (Ba 5p). However, the exact location of the peaks was found to be different in each experimental study. For example, the first peak was reported to be at 10, 11 and 12 eV in reflectance [7], characteristic energy loss [8] and XPS measurements [9, 10], respectively. In table 3, we therefore list the location of the peaks with reference to the first peak and compare them with the calculated values obtained in this study.

All of the experimental measurements yield the difference between the first two peaks to be about 2.5 eV, though they disagree in suggesting their origin. Based on the calculated band

Table 3. Interband transitions (in eV) in the cubic BaF_2.

Origin	Transition	This work	Reflectance spectra [7]	Energy-loss spectra [8]	Photoelectron spectra [9]
F(2p)	$\Gamma_{15}^{v} \rightarrow \Gamma_{1}^{c}$	0.00	0.00	0.0	0.0
	$X_{5}^{v} \rightarrow X_{1}^{c}$	2.2	2.6	2.4	2.5
	$X_{1}^{v} \rightarrow X_{1}^{c}$	3.4			
	$X_{1}^{v} \rightarrow X_{4}^{\prime c}$	3.6	3.5		
	$\Gamma_{15}^{v} \rightarrow \Gamma_{12}^{c}$	3.7			
	$X_{5}^{v} \rightarrow X_{2}^{c}$	4.3	4.3	4.2	
	$\Gamma_{25}^{\prime v} \rightarrow \Gamma_{12}^{c}$	5.3	5.3		
	$\Gamma_{25}^{\prime v} \rightarrow \Gamma_{25}^{\prime c}$	5.6			5.5
	$X_{1}^{v} \rightarrow X_{2}^{c}$	5.6			
	$X_{1}^{v} \rightarrow X_{5}^{c}$	6.1		5.8	
	$X_{1}^{v} \rightarrow X_{3}^{c}$	7.2	7.3		
Ba(5p)	$\Gamma_{8}^{v} \rightarrow \Gamma_{2}^{c}$	7.8	7.1	7.0	
	$X_{7}^{v} \rightarrow X_{1}^{c}$	9.7	9.9	9.3	9.0

Table 4. The calculated dielectric constant (ε) and refractive index (n) of BaF_2 in the cubic, orthorhombic and hexagonal phases.

BaF_2	Cubic	Orthorhombic	Hexagonal
ε_{xx}	2.012	2.364	2.267
ε_{yy}	2.012	2.177	2.267
ε_{zz}	2.012	2.651	2.391
n_{xx}	1.418	1.538	1.506
n_{yy}	1.418	1.475	1.506
n_{zz}	1.418	1.628	1.546

structure of the cubic BaF_2, we assign the interband transition from the top of the valence band to the bottom of the conduction band at Γ to the first peak and that at X to the second peak.

Assignments for the next three peaks originating from the upper valence band due to F 2p states are also listed in table 3. The temperature sensitive peak found in the reflectance spectra [7], which is about 3.50 eV away from the first excitation, is attributed to the excitation from the internal valence level to the conduction level close to its bottom edge ($X_{1}^{v} \rightarrow X_{4}^{\prime c}$). The unexplained shoulder, 7.30 eV away from the first excitation peak in the reflectance spectra [7], is attributed to excitation at X, from X_{1}^{v} to X_{3}^{c}.

For the interband transitions originating from the outermost core band due to Ba 5p states, the experimental measurements had identified two peaks at about 7 and 9 eV. Our calculated results attribute these peaks to be due to the interband excitations at Γ and X, respectively.

The optical dielectric constants of each phase of BaF_2 considered in this study were calculated by a sum over states (SOS) method using the LCAO–DFT crystalline functions obtained from electronic structure calculations. The details of the method have been described elsewhere [42]. Briefly, the electric dipolar Hamiltonian gauge was used with the length operator. It satisfies the Thomas–Reich–Kuhn rule concerning the sum over oscillator strengths from the core and valence bands to the conduction band which must be equal to the number of electrons per cell.

The values of ε are reported in table 4 for the three phases of BaF_2 together with their refractive indices. Because of the large bandgap of the cubic and high-pressure phases, the variation of the refractive index (n) with frequency was found to be smooth. For the cubic

BaF_2, the calculated value of (n) is 1.418 as compared to the value of 1.40 measured at $\lambda \simeq 10\ \mu$ [43, 44]. The mean value of the refractive index for the high-pressure phases is calculated to be higher than that of the cubic phase. For the metastable orthorhombic phase, both ε and n show a significant variation with respect to the symmetry axis. This is due to the low symmetry of the orthorhombic phase and has been observed [44] in the well known orthorhombic crystals of potassium titanyl phosphate (KTP).

6. Summary and conclusions

We have performed a first-principles study of BaF_2 in cubic, orthorhombic and hexagonal phases, predicting their structural, electronic and optical properties. In the cubic phase, calculations have provided assignments for several peaks associated with the interband transitions. In the high-pressure phases, calculations predict BaF_2 to be a direct-gap material. The calculated transition pressures from the cubic phase to the orthorhombic and hexagonal phases are in excellent agreement with values obtained from the high-pressure x-ray diffraction experiments.

Acknowledgment

The authors would like to thank Dr Aurora Costales for helpful discussions and her careful reading of the manuscript.

References

[1] Schmidt E D and Vedam K 1966 *J. Phys. Chem. Solids* **27** 1563
[2] Dutt N, Sharma O P and Shanker J 1985 *Phys. Status Solidi* **127** 67
[3] Kudrnovsky J, Christensen N E and Masek J 1991 *Phys. Rev.* B **43** 12597
[4] Kawano K *et al* 1999 *Phys. Rev.* B **60** 11984
[5] Jiang H *et al* 2000 *Phys. Rev.* B **62** 803
[6] Sata N, Eberman K, Eberl K and Maier J 2000 *Nature* **408** 946
[7] Rubloff G W 1972 *Phys. Rev.* B **5** 662
[8] Frandon J, Lahaye B and Pradal F 1972 *Phys. Status Solidi* b **53** 565
[9] Scrocco M 1985 *Phys. Rev.* B **32** 1301
[10] Miyahara T *et al* 1986 *J. Phys. Soc. Japan* **55** 408
[11] Gao Y, Tiedje T, Wong P C and Mitchell K A R 1993 *Phys. Rev.* B **48** 15578
[12] Tsujibayashi T *et al* 1999 *Phys. Rev.* B **60** R8442
[13] Poole R T *et al* 1976 *Phys. Rev.* B **13** 896
[14] Albert J P, Jouanin C and Gout C 1977 *Phys. Rev.* B **16** 925
[15] Heaton R A and Lin C C 1980 *Phys. Rev.* B **22** 3629
[16] Pandey R, Rérat M and Causa M 1999 *Appl. Phys. Lett.* **75** 4127
[17] Pandey R, Rérat M, Darrigan C and Causa M 2000 *J. Appl. Phys.* **88** 6462
[18] Minomura S and Drickamer H G 1961 *J. Chem. Phys.* **34** 670
[19] Catlow C R A, Norgett M J and Ross T A 1977 *J. Phys. C: Solid State Phys.* **10** 1627
[20] Zainullina V M, Zhukov V P and Zhukovsky V M 1998 *Phys. Status Solidi* b **210** 145
[21] Vail J M *et al* 1998 *Phys. Rev.* B **57** 764
[22] Andriessen J, Dorenbos P and Eijk C W E V 1991 *Mol. Phys.* **74** 535
[23] Ching W Y, Gan F and Huang M-Z 1995 *Phys. Rev.* B **52** 1596
[24] Samara G A 1970 *Phys. Rev.* B **2** 4194
[25] Leǵer J M, Haines J, Atouf A and Schulte O 1995 *Phys. Rev.* B **52** 13247
[26] Seifert V K F 1966 *Ber. Bunsenges. Phys. Chem.* **70** 1041
[27] Dandekar D P and Jamieson J C 1969 *Trans. Am. Crystallogr. Assoc.* **5** 19
[28] Leǵer J M, Haines J and Atouf A 1995 *Phys. Rev.* B **51** 3902
[29] Catti M *et al* 1991 *J. Phys.: Condens. Matter* **3** 4151

[30] Huzinaga S, McWilliams D and Cantu A A 1992 *Adv. Quantum Chem.* **97** 6504
[31] Becke A D 1988 *Phys. Rev.* A **38** 3098
[32] Perdew J P and Wang Y 1992 *Phys. Rev.* B **45** 13244
[33] Dovesi R, Roetti C and Saunders V R 1998 *CRYSTAL Program*
[34] Vinet P, Ferrante J and Smith J R 1941 *J. Phys. C: Solid State Phys.* **1**
[35] Lide D R (ed) 1996 *Handbook of Chemistry and Physics* (Boca Raton, FL: Chemical Rubber Company Press)
[36] Smyrl N R and Mamantov G 1978 *Adv. Inorg. Chem. Radiochem.* **21** 231
[37] Wagman D 1982 *J. Phys. Chem.* **11** 2
[38] Wyckoff R W G 1960 *Crystal Structures* vol 2 (New York: Interscience)
[39] Itoh M and Itoh H 1992 *Phys. Rev.* B **46** 15509
[40] Fiorentini V and Baldereschi A 1992 *J. Phys.: Condens. Matter* **4** 5967
[41] Samara G A 1975 *Phys. Rev.* B **10** 4529
[42] Ayma D, Campillo J P, Rérat M and Causá M 1997 *J. Comput. Chem.* **18** 1253
[43] Crystran http://www.crystran.co.uk/baf2data.htm
[44] Almaz Optics http://www.almazoptics.com/homepage/BaF2.htm